Nano Research

Open Access

Research Article

A strategy to improve the robustness of bound states in the continuum

Peiwen Ren, Zhuo Huang, Renxian Gao, Xiaoxiang Dong, Guoya Sun, Jian-Feng Li ✉, and Zhilin Yang ✉

College of Physical Science and Technology, State Key Laboratory of Physical Chemistry of Solid Surfaces, College of Chemistry and Chemical Engineering, College of Energy, Xiamen University, Xiamen 361005, China

Cite this article: *Nano Research*, **2025**, *18*, 94907132. https://doi.org/10.26599/NR.2025.94907132

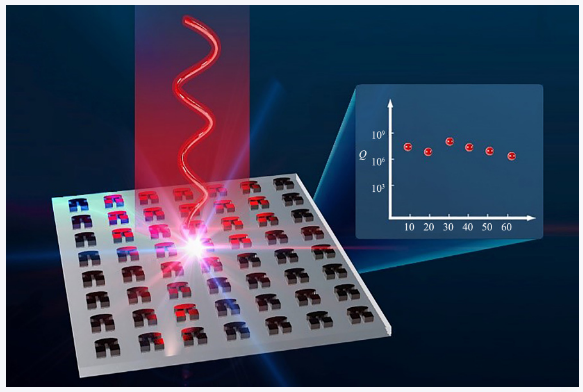

ABSTRACT: Bound states in the continuum (BICs) supported by dielectric metasurfaces have significantly propelled the progress in optical technologies, notably for manipulating potent light-matter interactions. However, achieving a robust quasi-BIC mode with high Q factor by adjusting geometric parameters remains a challenge, primarily the Q factors strongly depend on the asymmetric parameters and the stringent fabrication requirements. Here, we propose a novel strategy to enhance the robustness of the Q factor through the continuous excitation of the magnetic dipole mode with low energy loss. Through a specialized multi-cell structure, the nanoarrays can continuously excite the magnetic dipoles contributed by different structural components over a broad range of geometrical parameters, exhibiting exceptional robustness and high quality resonance. This work provides a theoretical scheme that offers new directions for obtaining robust high Q resonances and developing potential applications for high-performance optical devices.

KEYWORDS: bound states in the continuum (BICs), all-dielectric nanostructures, magnetic dipole, electric dipole, robust high Q factor

1 Introduction

The bound states in the continuum (BICs) are localized wave states with potentially infinite lifetimes and energies embedded in the continuous spectrum of radiating waves [1–6]. BICs have ultra-high quality electromagnetic resonance allowing for all-optical manipulation at the nanoscale, which substantially enhances the local electric field and facilitates light-matter interactions. The emergence of BICs has boosted fundamental research and applications of nano-optics, leading to many advances in the fields of optoelectronic integration and information processing [7–9]. Ideal BICs have an infinitely high Q factor, vanishing resonance width [10] and cannot be directly excited by far-field radiation. However, quasi-BICs have been proposed to allow for the leakage of small amounts of radiation into free space by adjusting the interference cancellation of different modes in the system [11]. This can be achieved by tuning the geometry [12] or excitation parameters of the quasi-BICs [13, 14]. By virtue of their outstanding features, such as ultra-narrow linewidth and ultra-strong local electromagnetic fields, quasi-BICs have been utilized in the construction of resonant metasurfaces for a range of applications, which include ultrasensitive hyperspectral imaging [15–17], lasers [18–20], catalytic metasurfaces [21], and nonlinear optical processes [22–25].

Recently, all-dielectric nanoresonators, governed by Mie-resonant nanoparticles, have emerged as a powerful tool to achieve quasi-BICs in finite structures [26, 27]. All-dielectric nanostructures not only avoid the inherent Ohmic loss of metal plasmas [28] but also can excite multiple types of electric and magnetic multilevel resonance modes [29–31]. The tight confinement of the strong electric fields and multiple interferences that are available in high-index dielectric nanostructures can lead to constructive or destructive interferences with unusual beam shapes, which offers novel opportunities to boost many optical effects [32, 33]. The magnetic dipole (MD) mode of high-index dielectric materials with low-loss characteristics is used in perfect magnetic mirrors [34], phase control [35], and enhanced optical nonlinearity [36].

Received: September 28, 2024; **Revised:** November 9, 2024
Accepted: November 12, 2024

✉Address correspondence to Jian-Feng Li, Li@xmu.edu.cn; Zhilin Yang, zlyang@xmu.edu.cn

Additionally, the spatial limited domain and near-field enhancement characteristics of the MD mode offer unique advantages in the strong local photoelectric field excitation of BICs, thus serving as a powerful tool for achieving high quality BIC resonance [37, 38]. Overall, the emergence of all-dielectric nanoresonators has significantly expanded the possibilities for designing novel optical devices based on quasi-BICs where their outstanding features, such as ultra-narrow linewidth and ultra-strong local electromagnetic fields, making them a promising avenue for various applications in nanophotonics and nanoelectronics.

In general, the excitation of sharp resonances in the BIC mode of all-dielectric systems often relies on stringent geometric configurations [39, 40], where the Q factor and near-field enhancement are highly sensitive to the geometrical parameters. This makes it particularly important to precisely and reproducibly control the structural parameters [41, 42]. Recently, the excitation of mirror magnetic dipoles [37] and proposal of different planar cutting methods [11] have both been effective in enhancing the Q factor of these structures. Besides, by adding a perturbed element to the unaltered BIC metasurface to enable coupling to radiation channels, the resulting metasurface supports high Q resonances by placing such elements close to a relevant high-symmetry point of the array [43]. Generally, the excitation conditions of high Q factor resonance always strongly depend on the structural configurations, which include the period, length, width, radius, thickness, etc. of the structure. Given the constraints of current fabrication techniques and the stringent application demands for high quality devices, there is an urgent need to design resonators that exhibit robustness to structural parameters. Here, robustness refers to the stability of the Q factor over a range of geometric parameters (e.g., length, gap, etc.).

In this study, we theoretically present a novel approach for achieving highly robust BIC resonances utilizing the low-loss magnetic dipole mode of all-dielectric materials. The specialized multi-unit structures support both electric dipole (ED) and magnetic dipole (MD) quasi-BIC resonance. Particularly, the nanoarrays can continuously excite low-loss magnetic dipoles using circular displacement currents contributed by different structural components. This mechanism provides a large structural tolerance for the excitation of magnetic dipole resonance, which greatly improves the robustness of the resonance. Extremely robust quality factors are achieved by leveraging a high refractive index all-dielectric MoS_2 nanostructure since the MD quasi-BIC is always accompanied by strong localized electric fields and ultra-narrow linewidths over a large range of geometric parameters. This design provides efficient theoretical support for designing high Q nanoarrays and opens up exciting prospects for exploring applications in biosensing, ultra-sensitive lasers, nonlinear optics, and quantum physics.

2 Models and principle

The physical model and basic regulation principle of the BIC resonance used for robustness research are shown in Fig. 1. The model is composed of periodic all-dielectric MoS_2 nanoarrays. MoS_2 has emerged as a promising class of novel materials for optoelectronics, which can be fabricated in a single step as dielectric radiative antennas due to high refractive index in visible and part of infrared [45]. Bulk MoS_2 has superiorities over conventional semiconductors because of its high refractive index and a relatively small imaginary part [46] which has a high density of light states and strong photon absorption capacity. Here, we consider a specialized multi-cell structure as a robust resonator. Each unit is composed of a specific elliptical cylinder where the long and short axes are defined as D_x and D_y, respectively, and a cubic nanoparticle pair with lengths and widths denoted as L and W, respectively, and h denotes the height of the nanoarray. Additionally, the distance between the nanocuboid pairs is referred to as the gap, P_x, and P_y represent the periodicity of the model system.

The basic physical principles used to improve the robustness of the BIC are shown in Figs. 1(b) and 1(c). The monolithic elliptical cylinders and cubes can excite closed toroidal displacement currents by governing specific geometrical parameters, which in turn

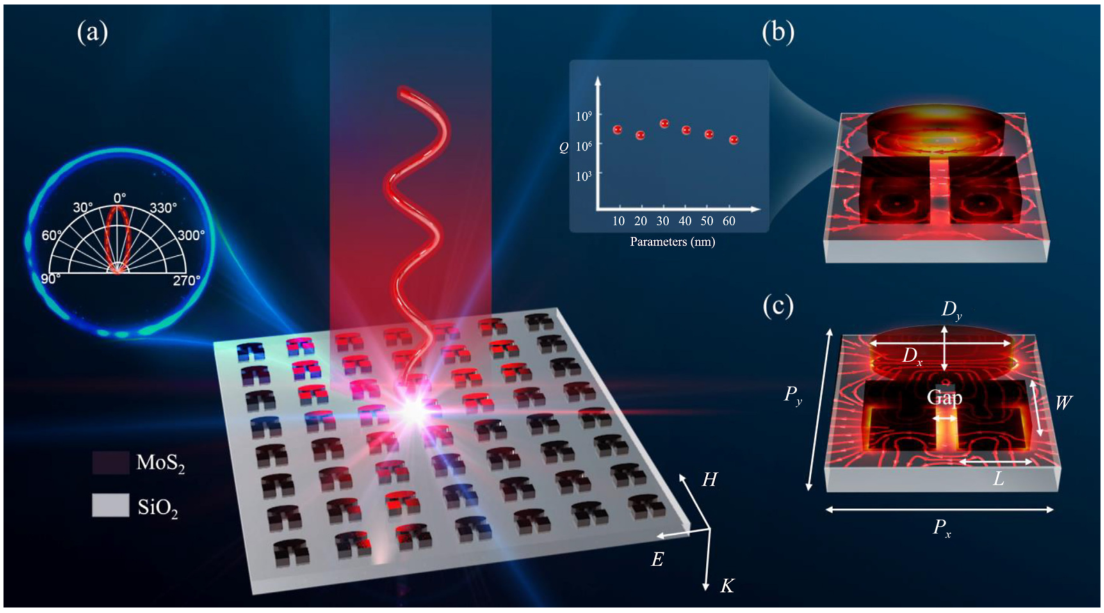

Figure 1 (a) Schematic illustration of a periodic all-dielectric nanoarray deposited on a quartz substrate, illuminated by x-polarized plane waves that propagate along the z-axis. (b) Schematic diagram of electric displacement vector distribution and the robustness of Q factors with different parameters of magnetic dipole mechanism. (c) Schematic diagram of electric displacement vector distribution of the electric dipole mechanism on the dielectric element.

generate low-loss magnetic dipoles. Our devised structure, shown in Fig. 1(b), is capable of exciting the magnetic dipole for both the upper elliptical cylinder and the lower nanocubic pair using different parameters, which regulates the geometric tolerance of the excitation conditions. In addition, the elliptical cylinder and nanocubic pair of the dielectric element can also excite the reversed ED moment, and the phase extinction interference between electric dipoles can induce the ED quasi-BICs mode, as shown in Fig. 1(c). Intriguingly, the nanoarrays are able to continuously excite low-loss magnetic dipoles through a specialized multi-cell structure design by regulating a series of geometric parameters for different structural components such as the axes length of the elliptical cylinder, the length of the paired cuboid and its "gap". Successive excitation of the MD resonance of different components circumvents the limitation that a single structure requires specific structural parameters to excite the magnetic modes and allows extremely robust high-Q BIC resonance within a wide range of structural tolerances.

Electromagnetic characteristics of the structure are investigated using the commercial software COMSOL Multiphysics. The nanoarray is illuminated by x-polarized plane waves propagating along the z-axis. In the calculation, the computation domain consists of only one unit cell without fabrication imperfections, and periodic conditions are employed to the four lateral boundaries in the x- and y-axis. In addition, a perfect matching layer (PML) is established above the metamaterial structure along the z-axis to eliminate the non-physical reflection at the boundary.

3 Results and discussion

To gain a deep insight into the physics of the high-quality BICs resonance in the asymmetry nanoarray, the transmission spectra and electric field enhancement for different geometrical parameters are demonstrated in Fig. 2. First, the transmission spectra of different gaps are calculated where the period of the unit is 550 nm ($P_x = P_y$), the structural thickness h is fixed as 100 nm, and the D_x and D_y of the upper elliptical cylinders are 360 and 125 nm, respectively. Two strong resonance modes (transmission dip) can be clearly seen in Fig. 2(a), and the blue shift is prominent as the gap increases (note: We have narrowed the wavelength range of the transmission spectrum and calculated its near-field enhancement in the illustration to clearly visualize the waveform of the ultra-narrow resonant peak and characterize its physical mechanism). From Fig. 2(a), it is obvious that increasing the gap distance causes a broadening in the linewidths corresponding to the ED quasi-BIC resonance, while the linewidths stimulated by MD quasi-BIC resonance mode remain ultra-narrow. The wavelengths and linewidths corresponding to the resonance modes at different gaps are shown in Fig. 2(c) (where the lengths of the bar of the longitudinal dotted lines represent the linewidths corresponding to the resonance peaks at different gaps). Here, the resonance peaks of the ED quasi-BIC resonance are gradually blueshifted and the linewidths are gradually broadened with the increase of gap. In contrast, magnetic resonance shows strong robustness to changes in gaps, always maintaining a small blueshift and narrow linewidth. From Fig. 2(b), the electric field intensity of the resonance dominated by the ED quasi-BIC resonance gradually decreases as the gap between the two cuboids increases. It is also worth noting that the order of magnitude of the electric field contributed by the MD quasi-BIC resonance remains essentially unchanged as the gap increases as shown by the trends displayed in Fig. 2(d).

To further investigate the physical origin of the two resonance modes, we studied the electric and magnetic field distribution under different modes. Benefiting from ingenious structural design, the nanoarrays can induce low-loss magnetic dipoles through circular displacement currents from various structural components. As illustrated in Figs. S1(a)–S1(c) in the Electronic Supplementary Material (ESM), the MD quasi-BIC mode excited by the annular displacement current can always be excited in the nanoarray even when the gap is increased and the contribution of the main magnetic mode is gradually transferred from the lower cuboid to the upper elliptical cylinder as the gap increases. Figure 3(a) describes the electric displacement vector distribution of MD resonance at a gap of 50 nm. The displacement vector on the

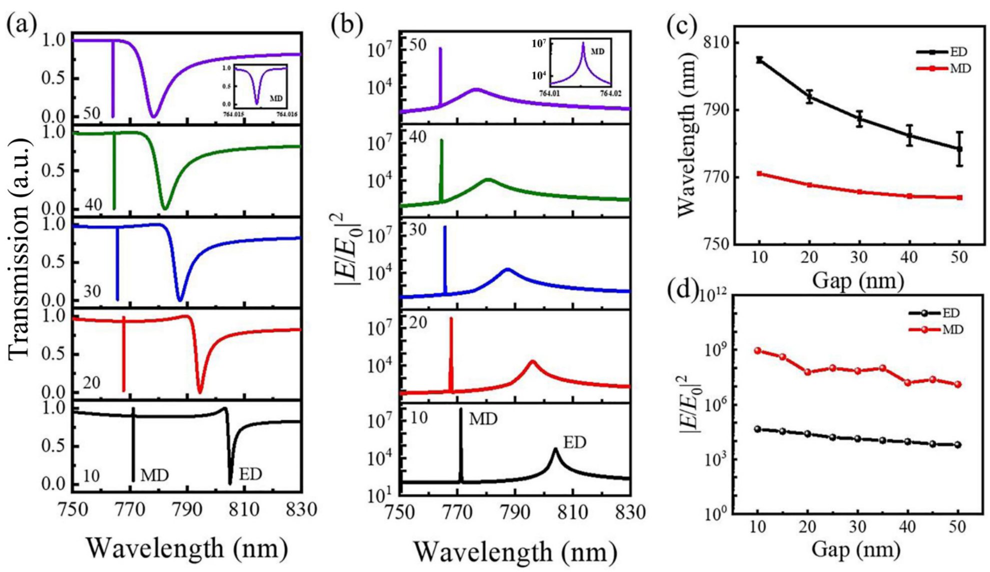

Figure 2 Analyses of the MD and ED quasi-BIC in the nanoarray with a period of 550 nm, an elliptical x- and y-axis of 360 and 125 nm, respectively. The height of 100 nm and the y-axis centers of the elliptical column and cubes are at P/4. (a) Evolution of the transmission spectra of MD and ED quasi-BIC at different gaps. (b) The corresponding local electric field enhancement with varying gaps. (c) Wavelength position of the MD and ED quasi-BIC formants at different gaps. The length of the bars represents the linewidth of the formant. (d) The intensity of the electric field enhancement as a function of the different gaps.

central cross-section of the x–y plane forms a closed annular displacement current generating a highly curved magnetic field, which leads to a strong magnetic field enhancement in the nanostructure (Fig. 3(c)), and matches the typical MD quasi-BIC mode. Moreover, the potential shift vector analysis diagram of the electric resonance BIC is also clearly visible. Figure 3(b) demonstrates the resonance waveform of ED quasi-BIC and its electromagnetic field distribution, which is the result of interference cancellation of the electric dipole moments of the nanoarray. Figures S1(d)–S1(f) in the ESM demonstrates that the electric dipole moment of the lower cuboid structure decreases gradually with the increase in the gap distance. This causes an increase in the energy radiated from the nanostructure and a decrease in the electric field strength. The calculations verify that the quasi-BICs resonance of the two modes is always accompanied by a strong local field in a wide range of gap variations. Apparently, profiting from the smaller radiation loss of the continuously magnetic dipole, the resonant local electric field enhancement has outstanding strong robustness.

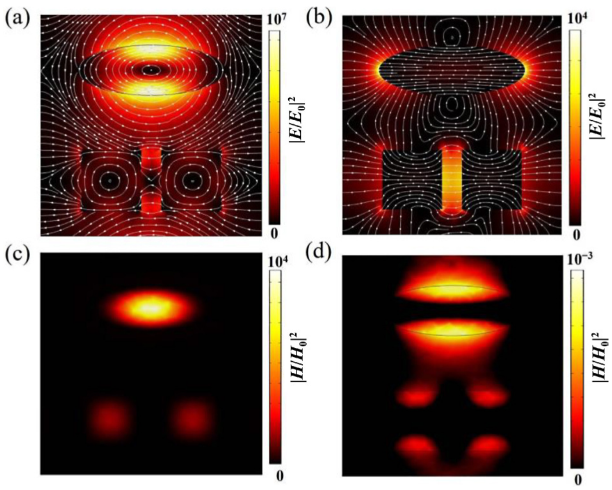

Figure 3 Electric and magnetic field distributions at the MD and ED quasi-BIC modes of the nanoarray. (a) Electric field distributions of the MD quasi-BIC resonance. (b) Electric field distributions of the ED quasi-BIC resonance. (c) Magnetic field distributions of the MD resonance. (d) Magnetic field distributions of the ED resonance.

The Cartesian multipole decomposition based on induced current density to calculate the scattering power of nanoarray is an effective method to analyze the specific physical mechanism. Generally, the oscillating charge current distribution in nanoarrays caused by the polarized plane wave of the incoming ray can be described as a series of electric, magnetic, and multiple polar moments. The Cartesian ED (***P***) and MD (***M***) moments can be calculated by the following formulae using the long-wavelength approximation [47]:

$$\boldsymbol{P} = \frac{1}{\mathrm{i}\omega}\int \boldsymbol{J}(\boldsymbol{r})\,\mathrm{d}^3\boldsymbol{r}$$

$$\boldsymbol{M} = \frac{1}{2c}\int \boldsymbol{r}\times\boldsymbol{J}(\boldsymbol{r})\,\mathrm{d}^3\boldsymbol{r}$$

where $\boldsymbol{r}$ is the position vector, c is the light velocity, and ω is the frequency. $\boldsymbol{J}(\boldsymbol{r})$ indicates the charge current in the structure. Here, $\boldsymbol{J}(\boldsymbol{r}) = -\mathrm{i}\omega\left(\varepsilon(\boldsymbol{r}) - \varepsilon_0 E(\boldsymbol{r})\right)$. ε denotes the dielectric constant of the material. Consequently, modifying the geometric length of the nanoparticles allows for an effective adjustment of the electric dipole moment. The scattered power of each dipole, I_{ED} and I_{MD} can be obtained by the following formulas [48–50]:

$$I_{\mathrm{MD}} = \frac{2\omega^4}{3c^3}|\boldsymbol{M}|^2$$

$$I_{\mathrm{ED}} = \frac{2\omega^4}{3c^3}|\boldsymbol{P}|^2$$

The corresponding multi-level decomposition in Fig. 4(a) confirms that the resonance mode of the structure is mainly dominated by the magnetic mode of the system; in contrast, the contributions of other models can be ignored. As illustrated in Figs. S2(a)–S2(c) in the ESM, the ingenious structural design permits the nanorod array to continuously excite low-loss magnetic dipoles through the contributions of different structural elements in the upper and lower parts and its contribution gradually shifts from the lower cuboid to the upper elliptical cylinder. Here, M_1 and M_2 represent the magnetic dipole moment excited by the upper elliptic cylinder and the lower cuboid, respectively. It is also worth noting that the Q factor of low-loss MD resonance is highly robust with Q-factors remaining above 10^6, as plotted in Fig. 4(c).

The multi-level decomposition of Fig. 4(b) confirms that the resonance mode of the corresponding ED quasi-BIC is mainly contributed by the interference cancellation of the two electric dipoles. Here, P_1 and P_2 represent the electric dipole moments excited by the upper elliptic cylinder and the lower cuboid, respectively. All the dotted lines are numerical simulations, as displayed in Fig. 4(d), for small values of the gap, the Q factors of the ED quasi-BIC present as an inverse quadratic. From Figs. S2(d)–S2(f), it can be summarized that as the asymmetric parameter of the cuboid gap increases, the radiation power P_2 of the lower dipole moment drops sharply. On account of the inability of P_1 and P_2 to achieve complete interference cancellation in the far field, the structure emits more energy into free space, which consequently leads to a decrease in its radiative Q factor and a broadening of its spectral linewidth.

To comprehensively verify our theoretical findings, elliptical cylinder arrays with different geometric parameters are also investigated. Similarly, the transmission spectrum, near-field enhancement, and the corresponding multipole contribution of the MD quasi-BIC and ED quasi-BIC with two cuboids for different L are calculated in Figs. S3(a)–S3(d) in the ESM (the gap fixed at 50 nm). The high Q in MD quasi-BIC further verifies the robustness of the system with respect to different structural parameters. In addition, the scattering power in Figs. S3(c) and S3(d) in the ESM at different L can elucidate the physical mechanism. The point-line diagram of numerical calculation in Fig. 5(b) indicates that a change in the lower cuboid L can also effectively excite low-loss magnetic modes in the structure. For ED quasi-BIC resonance in Fig. 5(b), it is evident that the Q factor is gradually enhanced with the increase of L. This phenomenon can be attributed to the relationship between the radiation loss and the dipole moment (P_2). As shown in Fig. S2 in the ESM, an increase in L leads to a corresponding increase in P_2, which signifies a reduction in the disparity between P_2 and P_1, thus reducing the radiation loss associated with the resonant mode. Next, different long and short-axis diameters of elliptical cylinders are regulated, the nanoarray that has a large geometric range would also support such ED and MD quasi-BIC modes and this process is accompanied by strong resonance and large field enhancement

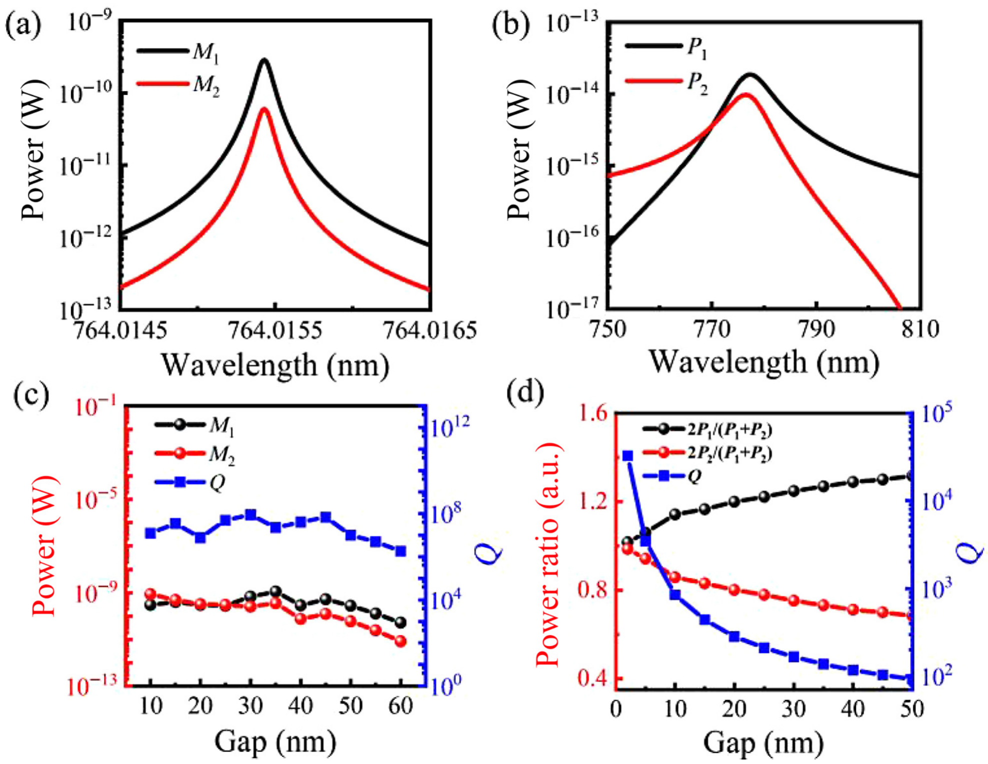

Figure 4 (a) and (b) The normalized Cartesian multipole decomposition results of MD and ED quasi-BIC with gaps set to 50 nm. (c) Calculated maximum high Q factors (blue) and radiated power of MD quasi-BIC excited by elliptical cylinder (black) and cuboids (red) with different gaps. (d) Calculated maximum high Q factors (blue) and radiated power of ED quasi-BIC excited by elliptical cylinder (black) and cubes (red) with different gaps.

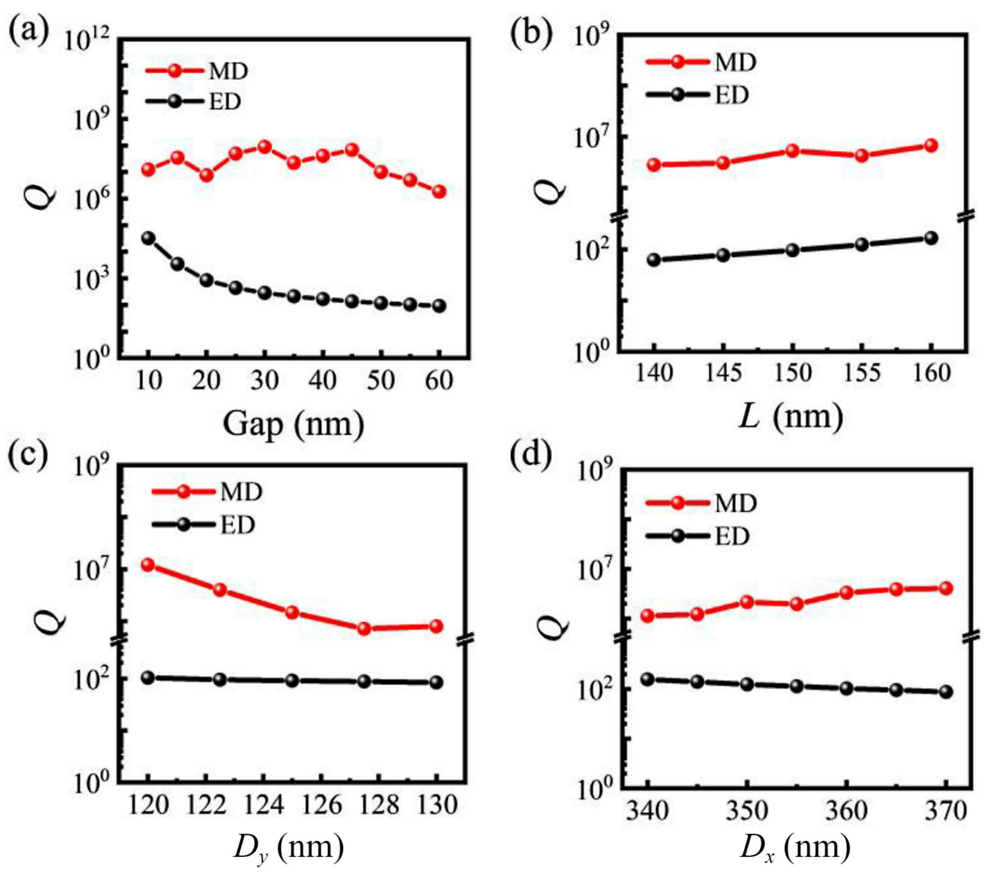

Figure 5 Analyses of the MD and ED quasi-BIC with different D_x and D_y using a period of 550 nm, the height of 100 nm. (a) The calculated Q factor of MD and ED quasi-BIC with different gaps. When gap is fixed at 50 nm, the calculated Q factor of MD and ED quasi-BIC with different L (b), D_y (c), and D_x (d).

(Figs. S4(a) and S4(b) in the ESM). From the plot in Figs. 5(c) and 5(d), it is clear that changing the parameters D_y and D_x has a negligible effect on the high Q factor of the MD resonance, suggesting that these structures are stable for a wide range of geometric parameters. Similarly, by utilizing a specialized multi-cell structure design, the nanoarrays are capable of continuously exciting low-loss magnetic dipoles through circular displacement currents contributed by various structural components, which can once again confirm that the magnetic structure of the BIC can significantly reduce the scattering loss and improve the robustness. As illustrated in Fig. 5(c), the Q factor trend of the ED quasi-BIC exhibits a relatively stable pattern as D_y changes. This stability is due to the limited influence of D_y on the dipole moment over a small range of geometric parameter variations. As depicted in Fig. 5(d), the Q factor for the ED quasi-BIC diminishes as the length of D_x grows. This occurs because the elevation of D_x results in an increase of P_1, amplifying the disparity between the upper and lower electric dipole moments. Consequently, this pronounced difference leads to a reduction in the Q value of the resonance mode.

4 Conclusions

In summary, we have theoretically presented a novel approach for developing highly robust BIC resonances utilizing the low-loss magnetic dipole mode of all-dielectric nanoarrays. The specialized multi-unit structures support both ED and MD resonance. Particularly, the continuous excitation of low-loss MD resonance via circular displacement currents from various structural components resulting in strong robustness and high-quality BIC resonances over a wide range of geometric parameters. A clear physical mechanism has been proven by analyzing near-field coupling and multi-level decomposition. Additionally, an ultra-high Q factor (~ 10^7) under normal excitation was demonstrated by utilizing MD resonances, where radiative losses are greatly suppressed. The MD with a high Q factor is remarkably robust against geometric defects over a wide range of parameters providing the groundwork towards smart engineering of resonances in metaoptics for nonlinear nanophotonics, ultrafast active metadevices and optoelectronic devices.

Electronic Supplementary Material: Supplementary material (simulation method; simulation results of electric fields of MD quasi-BIC and ED quasi-BIC with different gaps; simulation results of normalized Cartesian multipole decomposition results of MD quasi-BIC and ED quasi-BIC with different gaps; simulation results of the transmission spectra, the electric field enhancement and point plot of Q values of the system with different L; simulation results of transmission spectra of the MD quasi-BIC and ED quasi-BIC with different D_x and D_y) is available in the online version of this article at https://doi.org/10.26599/NR.2025.94907132.

Data availability

All data needed to support the conclusions in the paper are presented in the manuscript and the ESM. Additional data related to this paper may be requested from the corresponding author upon request.

Acknowledgements

This work was supported by the National Key Research and Development Program of China (No. 2021YFA1201502), Scientific and Technological Innovation 2030-"Quantum Communication and quantum computer" Major Project (No. 2023ZD0300304) and the National Natural Science Foundation of China (Nos. 92161118, 12174324, and 21925404)

Declaration of competing interest

All the contributing authors report no conflict of interests in this work.

Author contribution statement

P. W. R.: Data curation, validation, writing manuscript, models and principle design, writing manuscript. Z. H., R. X. G., X. X. D., and G. Y. S.: Validation and writing manuscript. Z. L. Y. and J.-F. L.: Data curation, validation, project administration, funding acquisition. All the authors have approved the final manuscript.

Use of AI statement

None.

References

[1] Kühner, L.; Sortino, L.; Berté, R.; Wang, J.; Ren, H. R.; Maier, S. A.; Kivshar, Y.; Tittl, A. Radial bound states in the continuum for polarization-invariant nanophotonics. *Nat. Commun.* **2022**, *13*, 4992.

[2] Kang, M.; Zhang, S. P.; Xiao, M.; Xu, H. X. Merging bound states in the continuum at off-high symmetry points. *Phys. Rev. Lett.* **2021**, *126*, 117402.

[3] Deriy, I.; Toftul, I.; Petrov, M.; Bogdanov, A. Bound states in the continuum in compact acoustic resonators. *Phys. Rev. Lett.* **2022**, *128*, 084301.

[4] Marinica, D. C.; Borisov, A. G.; Shabanov, S. V. Bound states in the continuum in photonics. *Phys. Rev. Lett.* **2008**, *100*, 183902.

[5] Plotnik, Y.; Peleg, O.; Dreisow, F.; Heinrich, M.; Nolte, S.; Szameit, A.; Segev, M. Experimental observation of optical bound states in the continuum. *Phys. Rev. Lett.* **2011**, *107*, 183901.

[6] Hsu, C. W.; Zhen, B.; Lee, J.; Chua, S. L.; Johnson, S. G.; Joannopoulos, J. D.; Soljačić, M. Observation of trapped light within the radiation continuum. *Nature* **2013**, *499*, 188–191.

[7] Tian, J. Y.; Luo, H.; Li, Q.; Pei, X. L.; Du, K. K.; Qiu, M. Near-infrared super-absorbing all-dielectric metasurface based on single-layer germanium nanostructures. *Laser Photon. Rev.* **2018**, *12*, 1800076.

[8] Fan, K. B.; Suen, J. Y.; Liu, X. Y.; Padilla, W. J. All-dielectric metasurface absorbers for uncooled terahertz imaging. *Optica* **2017**, *4*, 601–604.

[9] Hu, P.; Wang, J. J.; Jiang, Q.; Wang, J.; Shi, L.; Han, D. Z.; Zhang, Z. Q.; Chan, C. T.; Zi, J. Global phase diagram of bound states in the continuum. *Optica* **2022**, *9*, 1353–1361.

[10] Koshelev, K.; Lepeshov, S.; Liu, M. K.; Bogdanov, A.; Kivshar, Y. Asymmetric metasurfaces with high-*Q* resonances governed by bound states in the continuum. *Phys. Rev. Lett.* **2018**, *121*, 193903.

[11] Liu, Z. J.; Xu, Y.; Lin, Y.; Xiang, J.; Feng, T. H.; Cao, Q. T.; Li, J. T.; Lan, S.; Liu, J. High-*Q* quasibound states in the continuum for nonlinear metasurfaces. *Phys. Rev. Lett.* **2019**, *123*, 253901.

[12] Koshelev, K.; Tang, Y. T.; Li, K.; Choi, D. Y.; Li, G. X.; Kivshar, Y. Nonlinear metasurfaces governed by bound states in the continuum. *ACS Photonics* **2019**, *6*, 1639–1644.

[13] Liang, Y.; Koshelev, K.; Zhang, F. C.; Lin, H.; Lin, S. R.; Wu, J. Y.; Jia, B. H.; Kivshar, Y. Bound states in the continuum in anisotropic plasmonic metasurfaces. *Nano Lett.* **2020**, *20*, 6351–6356.

[14] Romano, S.; Mangini, M.; Penzo, E.; Cabrini, S.; De Luca, A. C.; Rendina, I.; Mocella,V.; Zito, G. Ultrasensitive surface refractive index imaging based on quasi-bound states in the continuum. *ACS Nano* **2020**, *14*, 15417–15427.

[15] Murai, S.; Abujetas, D. R.; Castellanos, G. W.; Sánchez-Gil, J. A.; Zhang, F. F.; Rivas, J. G. Bound states in the continuum in the visible emerging from out-of-plane magnetic dipoles. *ACS Photonics* **2020**, *7*, 2204–2210.
[16] Jahani, Y.; Arvelo, E. R.; Yesilkoy, F.; Koshelev, K.; Cianciaruso, C.; De Palma, M.; Kivshar, Y.; Altug, H. Imaging-based spectrometer-less optofluidic biosensors based on dielectric metasurfaces for detecting extracellular vesicles. *Nat. Commun.* **2021**, *12*, 3246.
[17] Yesilkoy, F.; Arvelo, E. R.; Jahani, Y.; Liu, M. K.; Tittl, A.; Cevher, V.; Kivshar, Y.; Altug, H. Ultrasensitive hyperspectral imaging and biodetection enabled by dielectric metasurfaces. *Nat. Photonics* **2019**, *13*, 390–396.
[18] Wang, Y. H.; Fan, Y. B.; Zhang, X. D.; Tang, H. J.; Song, Q. H.; Han, J. C.; Xiao, S. M. Highly controllable etchless perovskite microlasers based on bound states in the continuum. *ACS Nano* **2021**, *15*, 7386–7391.
[19] Hwang, M. S.; Lee, H. C.; Kim, K. H.; Jeong, K. Y.; Kwon, S. H.; Koshelev, K.; Kivshar, Y.; Park, H. G. Ultralow-threshold laser using super-bound states in the continuum. *Nat. Commun.* **2021**, *12*, 4135.
[20] Kodigala, A.; Lepetit, T.; Gu, Q.; Bahari, B.; Fainman, Y.; Kanté, B. Lasing action from photonic bound states in continuum. *Nature* **2017**, *541*, 196–199.
[21] Hu, H. Y.; Weber, T.; Bienek, O.; Wester, A.; Hüttenhofer, L.; Sharp, I. D.; Maier, S. A.; Tittl, A.; Cortés, E. Catalytic metasurfaces empowered by bound states in the continuum. *ACS Nano* **2022**, *16*, 13057–13068.
[22] Bijloo, F.; Murzyn, K.; van Emmerik, F.; den Boef, A. J.; Kraus, P. M.; Koenderink, A. F. Near-unity all-optical modulation of third-harmonic generation with a Fano-resonant dielectric metasurface. *Nano Lett*. **2024**, *24*, 12942–12947.
[23] Bernhardt, N.; Koshelev, K.; White, S. J. U.; Meng, K. W. C.; Fröch, J. E.; Kim, S.; Tran, T. T,; Choi, D. Y,; Kivshar, Y.; Solntsev, A. S.. Quasi-BIC resonant enhancement of second-harmonic generation in WS_2 monolayers. *Nano Lett.* **2020**, *20*, 5309–5314.
[24] Koshelev, K.; Kruk, S.; Melik-Gaykazyan, E.; Choi, J. H.; Bogdanov, A.; Park, H. G.; Kivshar, Y. Subwavelength dielectric resonators for nonlinear nanophotonics. *Science* **2020**, *367*, 288–292.
[25] Park, J. S.; Li, C. T.; Kim, K. H.; Tang, Y. K.; Murphey, C. G. E.; Teitsworth, T. S.; Kim, S.; Harutyunyan, H.; Cahoon, J. F. Optical nonlinearity in silicon nanowires enabled by bound states in the continuum. *ACS Nano* **2023**, *17*, 11729–11738.
[26] Staude, I.; Schilling, J. Metamaterial-inspired silicon nanophotonics. *Nat. Photonics* **2017**, *11*, 274–284.
[27] Koshelev, K.; Bogdanov, A.; Kivshar, Y. Meta-optics and bound states in the continuum. *Sci. Bull.* **2019**, *64*, 836–842.
[28] Campione, S.; Liu, S.; Basilio, L. I.; Warne, L. K.; Langston, W. L.; Luk, T. S.; Wendt, J. R.; Reno, J. L.; Keeler, G. A.; Brener, I. et al. Broken symmetry dielectric resonators for high quality factor fano metasurfaces. *ACS Photonics* **2016**, *3*, 2362–2367.
[29] Fu, Y. H.; Kuznetsov, A. I.; Miroshnichenko, A. E.; Yu, Y. F.; Luk' yanchuk, B. Directional visible light scattering by silicon nanoparticles. *Nat. Commun.* **2013**, *4*, 1527.
[30] Evlyukhin, A. B.; Novikov, S. M.; Zywietz, U.; Eriksen, R. L.; Reinhardt, C.; Bozhevolnyi, S. I.; Chichkov, B. N. Demonstration of magnetic dipole resonances of dielectric nanospheres in the visible region. *Nano Lett.* **2012**, *12*, 3749–3755.
[31] Yang, C. Y.; Yang, J. H.; Yang, Z. Y.; Zhou, Z. X.; Sun, M. G.; Babicheva, V. E.; Chen, K. P. Nonradiating silicon nanoantenna metasurfaces as narrowband absorbers. *ACS Photonics* **2018**, *5*, 2596–2601.
[32] Carletti, L.; Koshelev, K.; De Angelis, C.; Kivshar, Y. Giant nonlinear response at the nanoscale driven by bound states in the continuum. *Phys. Rev. Lett.* **2018**, *121*, 033903.
[33] Kruk, S.; Kivshar, Y. Functional meta-optics and nanophotonics governed by mie resonances. *ACS Photonics* **2017**, *4*, 2638–2649.
[34] Liu, S.; Sinclair, M. B.; Mahony, T. S.; Jun, Y. C.; Campione, S.; Ginn, J.; Bender, D. A.; Wendt, J. R.; Ihlefeld, J. F.; Clem, P. G. et al. Optical magnetic mirrors without metals. *Optica* **2014**, *1*, 250–256.
[35] Decker, M.; Staude, I.; Falkner, M.; Dominguez, J.; Neshev, D. N.; Brener, I.; Pertsch, T.; Kivshar, Y. S. High-efficiency dielectric Huygens' surfaces. *Adv. Opt. Mater.* **2015**, *3*, 813–820.
[36] Shcherbakov, M. R.; Vabishchevich, P. P.; Shorokhov, A. S.; Chong, K. E.; Choi, D. Y.; Staude, I.; Miroshnichenko, A. E.; Neshev, D. N.; Fedyanin, A. A.; Kivshar, Y. S. Ultrafast all-optical switching with magnetic resonances in nonlinear dielectric nanostructures. *Nano Lett.* **2015**, *15*, 6985–6990.
[37] Yang, G. C.; Dev, S. U.; Allen, M. S.; Allen, J. W.; Harutyunyan, H. Optical bound states in the continuum enabled by magnetic resonances coupled to a mirror. *Nano Lett.* **2022**, *22*, 2001–2008.
[38] Tian, J. Y.; Li, Q.; Belov, P. A.; Sinha, R. K.; Qian, W. P.; Qiu, M. High-Q all-dielectric metasurface: Super and suppressed optical absorption. *ACS Photonics* **2020**, *7*, 1436–1443.
[39] Anthur, A. P.; Zhang, H. Z.; Paniagua-Dominguez, R.; Kalashnikov, D. A.; Ha, S. T.; Maß, T. W. W.; Kuznetsov, A. I.; Krivitsky, L. Continuous wave second harmonic generation enabled by quasi-bound-states in the continuum on gallium phosphide metasurfaces. *Nano Lett.* **2020**, *20*, 8745–8751.
[40] Sinev, I. S.; Koshelev, K.; Liu, Z. J.; Rudenko, A.; Ladutenko, K.; Shcherbakov, A.; Sadrieva, Z.; Baranov, M.; Itina, T.; Liu, J. et al. Observation of ultrafast self-action effects in quasi-BIC resonant metasurfaces. *Nano Lett.* **2021**, *21*, 8848–8855.
[41] Cao, F. Z.; Zhou, M. M.; Cheng, C. W.; Li, H. J.; Jia, Q. W.; Jiang, A. W.; Lyu, B.; Liu, D. H.; Han, D. Z; Gwo, S. et al. Interaction of plasmonic bound states in the continuum. *Photon. Res.* **2023**, *11*, 724–731.
[42] You, S.; He, H. X.; Zhang, Y.; Duan, H.; Wang, L. L.; Wang, Y. Y.; Luo, S. Y.; Zhou, C. B. Resonance wavelength stabilization of quasi-bound states in the continuum constructed by symmetry breaking and area compensation. *Nano Lett.* **2024**, *24*, 15300–15307.
[43] Moretti, G. Q.; Tittl, A.; Cortés, E.; Maier, S. A.; Bragas, A. V.; Grinblat, G. Introducing a symmetry-breaking coupler into a dielectric metasurface enables robust high-Q quasi-BICs. *Adv. Photonics Res.* **2022**, *3*, 2200111.
[44] Jin, J. C.; Yin, X. F.; Ni, L. F.; Soljačić, M.; Zhen, B.; Peng, C. Topologically enabled ultrahigh-Q guided resonances robust to out-of-plane scattering. *Nature,* **2019**, *574*, 501–504.
[45] Verre, R.; Baranov, D. G.; Munkhbat, B.; Cuadra, J.; Käll, M.; Shegai, T. Transition metal dichalcogenide nanodisks as high-index dielectric Mie nanoresonators. *Nat. Nanotechnol.* **2019**, *14*, 679–683.
[46] Ermolaev, G. A.; Stebunov, Y. V.; Vyshnevyy, A. A.; Tatarkin, D. E.; Yakubovsky, D. I.; Novikov, S. M.; Baranov, D. G.; Shegai, T.; Nikitin, A. Y.; Arsenin, A. V. Broadband optical properties of monolayer and bulk MoS_2. *npj 2D Mater. Appl.* **2020**, *4*, 21.
[47] Radescu, E. E.; Vaman, G. Exact calculation of the angular momentum loss, recoil force, and radiation intensity for an arbitrary source in terms of electric, magnetic, and toroid multipoles, *Phys. Rev. E* **2002**, *65*, 046609.
[48] Wang, R.; Negro, L. D. Engineering non-radiative anapole modes for broadband absorption enhancement of light. *Opt. Express* **2016**, *24*, 19048–19062.
[49] Li, S. Y.; Zhou, C. B.; Liu, T. T.; Xiao, S. Y. Symmetry-protected bound states in the continuum supported by all-dielectric metasurfaces, *Phys. Rev. A* **2019**, *100*, 063803.
[50] Wang, J. Y.; Yang, W. M.; Sun, G. Y.; He, Y. L.; Ren, P. W.; Yang, Z. L. Boosting anapole-exciton strong coupling in all-dielectric heterostructures. *Photonics Res.* **2022**, *10*, 7.